Matching analysis of mixed matrix membranes for organic solvent reverse osmosis

Conrad Roos, Dylan Weber, Hye Youn Jang, Ryan P. Lively*

School of Chemical and Biomolecular Engineering, College of Engineering, Georgia Institute of Technology, Atlanta, GA, 30332, USA

1. Abstract

Existing polymeric membranes struggle to separate small molecule solvents in the liquid phase due to low selectivity from solvent-induced plasticization and dilation. Mixed matrix membranes (MMM) can potentially alleviate this issue via diffusion-based separations within rigid framework materials. Previous work from our lab and others has shown that organic solvent reverse osmosis membranes have different responses to transmembrane pressure depending on whether the material is a rigid structure (e.g., a carbon, zeolite, or metal-organic framework) or a swollen polymer. This work combines two Maxwell-Stefan transport models, representing the flexible polymer phase and a rigid microporous filler, with the Maxwell model to predict mixed matrix membrane solvent separation performance as a function of pressure and membrane material properties. The model demonstrates that for every filler perm-selectivity, there is a filler permeability that provides the largest separation factor in the final MMM. This optimum permeability increases with the filler's perm-selectivity. Dual-layer UiO-66/Matrimid® hollow fiber MMMs were created to evaluate the model's prediction on the influence of transmembrane pressure on the separation of toluene and mesitylene as a test case. The UiO-66/Matrimid® membrane demonstrated a predicted decline in permeance as pressure was increased. The separation factors increased as higher pressures raised the driving force for separation, consistent with the model. UiO-66 was shown to have superior selectivity to Matrimid® in toluene/mesitylene; however, we conclude that ultra-selective materials are ultimately needed to enable the mixed matrix membrane concept for the most challenging solvent-solvent separations, and open questions remain about polymer-filler pairings for organic solvent reverse osmosis.

2. Introduction

The separation and purification of organic liquids are critical to a wide range of industries. The majority of these separations occur through highly engineered thermal separations.¹ While these processes are highly proficient at their respectful separations; they demand a tremendous amount of energy.² The desire to increase throughput while reducing energy demands has strengthened interest in alternate separation technologies that can potentially augment existing separation systems. As one of these technologies, membranes offer the potential to reduce separation energy intensity.³ This reduction is due to an avoidance of a thermal phase change. While membranes are unlikely to fully displace the current thermal separation technologies, substantial energy savings may be realized through hybrid processes where membranes are paired with a thermal separation.⁴⁻⁵ While membranes have seen widespread success in water purification and commercialization in organic solvent nanofiltration, there still exists an opportunity for practical membranes targeting nonaqueous liquid phase small molecule separations.

Currently, polymeric membranes represent the majority of commercially-available technologies. These membranes are continuous polymeric matrices and benefit from relatively low costs and ease of production. While these membranes have seen commercial success, they are not without their drawbacks, including an inherent tradeoff between permeability and selectivity, along with a propensity to plasticize when challenged with strongly condensable species (such as solvents). Plasticization is the result of interactions between the penetrant and the polymeric matrix and occurs when these interactions increase polymer chain mobility. This increased mobility boosts the membrane's permeability while dramatically reducing its selectivity. An effective tool against plasticization is polymer cross-linking. Chemical cross-linking is one method to inhibit chain mobility and reduce polymer dilation. This effect has been observed in both gas and liquid separations. This work utilizes chemical cross-linking of hollow fiber membranes using a diamine linker, which has previously been demonstrated as an effective stabilization approach for solvent separations.

While cross-linking is a facile method to inhibit polymer dilation, inorganic membranes avoid dilation as well as plasticization and demonstrate superior separation performance. The boost in performance comes with a tradeoff in both cost and ease of fabrication and handling. A third class of membranes, mixed matrix membranes (MMM), combine the relatively low cost and ease of fabrication from polymeric membranes with the superior performance of inorganic membranes. To accomplish this, inorganic particles are dispersed throughout a continuous polymeric matrix, creating a membrane that can break past the inherent permeability/selectivity tradeoff found with polymeric membranes. Inorganic membranes' vast range of sorption and diffusion properties allow for nearly endless customization of a mixed matrix membrane's properties. Leveraging this customizability into a specialized membrane requires understanding how the inorganic filler's properties and operational parameters influence the MMM.

The fundamental underpinnings of transport in organic solvent reverse osmosis (OSRO) are shared with aqueous RO membranes and were developed simultaneously. Transport in OSRO abides by a solution-diffusion method of permeation, where transport is not driven by an internal pressure gradient but by a pressure-induced activity gradient. A major implication of an activity driving force is the system's non-linear increase in flux as pressure increases. This stems from the existence of a finite driving force, as the solvent activity within the membrane is intrinsically linked to the volumetric loading of the solvent. The physical limits of volume loading place a physical limit on the driving force. As solution-diffusion transport occurs once transport departs from continuum fluid flow, the penetrant-membrane interactions are a key factor in OSRO performance. For microporous materials, the pore size is a key characteristic as it primarily determines the speed of diffusion through the material, while functional groups, open metal sites, material composition, and other sources of penetrant-membrane attraction clearly have an important role in shaping OSRO performance. While in polymers, chain mobility and resistance to swelling play the foremost role in determining diffusion speed of the penetrants, with functional groups and

chemical characteristics of the repeat units (aromatics, electron distribution, etc.) play a role in the sorption of penetrants on the membrane.

As research in OSRO membranes has expanded so have the materials that have demonstrated successful OSRO separations, including carbon molecular sieves, ¹³ and polymers. ¹⁴ Recently, some of these materials have been fabricated in a commercially scalable hollow fiber membrane morphology. ¹⁵⁻¹⁶ There have been no successful demonstrations of a mixed matrix membrane separating small molecule organic solvents in the OSRO regime that we know of; our aim here is to describe the fundamental issues associated with polymer-filler pairing and experimentally demonstrate a workable mixed matrix OSRO membrane.

While the membrane composition is critical, its morphology can be the deciding factor in its commercial appeal. Currently, there are two morphologies with widespread use: spiral wound and hollow fiber. Here, a hollow fiber morphology is utilized, which creates a higher surface area to volume ratio than spiral wound systems.⁷ These membranes are fabricated through non-solvent induced phase separation, creating fibers with a dense outer skin layer, which performs the separation, supported by an interpenetrating porous substructure that provides mechanical stability without appreciable mass transfer resistance. These benefits have attracted much attention in the area of gas separations, while less work has focused on applying this morphology towards organic solvent separations, although a few notable examples exist. 17-19 Here, the spinning protocol for a MOF/Matrimid® hollow fiber membrane was adapted from work done by Clausi and Koros.²⁰ Unlike their previous work, which utilized a single pure polymer dope, this work utilized a technique known as dual-layer spinning, which has been used to fabricate MMMs for gas separations.²¹⁻²³ As opposed to more traditional hollow fiber spinning where a single polymeric dope is used, dual-layer spinning utilizes a sheath layer to surround the core. This second sheath dope allows for independent tuning of both dopes and the restriction of expensive inorganic particles to only the sheath dope, reducing the amount of inorganic material necessary for membrane fabrication.

Fabricating novel mixed matrix membranes is a time-intensive process, and there is always the risk that the material pairing is unsuitable for the targeted separation. This work seeks to utilize transport models that require minimal experimental information, to analyze MMMs for OSRO separations. Beyond this, we are interested in understanding how the properties of the polymer and filler affect the performance of the MMM. This analysis will focus on material properties (both polymer and filler) with the objective of furthering our understanding of optimizing mixed matrix membranes for targeted separations. To test the model's predictions, UiO-66/Matrimid® mixed matrix membranes were fabricated as dual-layer hollow fibers. UiO-66 and Matrimid® were chosen as they are well characterized and easily acquired, allowing other laboratories to easily recreate the MMMs in this work. These membranes are used in a test separation of toluene and mesitylene. These results are compared to the Maxwell-Stefan-derived transport to improve understanding of mixed matrix membrane behavior within the organic solvent reverse osmosis regime.

3. Theory

3.1 Polymer Transport

Solvent permeation in the OSRO regime through non-porous amorphous glassy polymers has been shown to follow solution-diffusion or sorption-diffusion in both polymeric and microporous materials.²⁴ This model states that the pressure within the membrane is constant and that permeation is driven not by a pressure gradient but by an activity or concentration gradient. This transition from a pressure-driven process to an activity-driven process occurs as the effective pore size of the materials shrinks. The breakdown of continuum flow necessary for a pressure-driven pore flow method of transport has been shown to occur as the pore size approaches approximately 2-3x the smallest molecular cross-section of the solvent molecule.²⁵ The resultant solution-diffusion permeability is commonly described as the product of diffusive and sorption contributions, shown in equation 1, allowing a straightforward method of approaching membrane transport.

$$\mathbb{P} = D \times \mathbb{S} \tag{1}$$

Where \mathbb{P} is the permeability, D refers to the Fickian diffusivity, and \mathbb{S} represents the sorption coefficient.

While Fickian diffusivities in Equation 1 are relatively straightforward to measure and provide good predictions of single component permeation, multicomponent systems commonly present large deviations from Fickian behavior. The Maxwell-Stefan model for transport provides a more robust method for multicomponent systems. A benefit of the Maxwell-Stefan framework is that its diffusivities are nominally concentration independent, unlike Fickian diffusivities. The Maxwell-Stefan formula, with constant temperature and pressure, is:²⁶

$$-\nabla_{T}\mu_{i} = -\nabla\mu_{i}|_{T,P} = RT \sum_{\substack{j=1\\i\neq i}}^{n} \frac{x_{j}(u_{i}-u_{j})}{\Theta_{ij}}, i = 1,2,...,n$$
(2)

Where μ_i is the chemical potential, x_j is the mole fraction, u_i is the species velocity, and D_{ij} is the Maxwell-Stefan diffusivity for a specific pair. While molar compositions can work well in rigid microporous systems, they become difficult to quantify in polymer systems due to the ill-defined molecular weight distribution of polymer chains. Alternative measures of composition have been used, including weight fractions, $^{27-28}$ but volume fractions are more physically meaningful. Heintz and Stephan first replaced measures of molar composition with volume fractions. 29 This switch provided the additional benefit of aligning the Maxwell-Stefan equations closer to the Flory-Huggins model, which is a common thermodynamic sorption model for polymer solutions. A drawback of this updated model is an assumption that the exchange coefficients are reciprocal, and without accounting for the conversion of volume fractions this reciprocity causes the model to not satisfy the Gibbs-Duhem equation. 30

Fornasiero, Prausnitz, and Radke addressed this problem by creating an updated Maxwell-Stefan equation that satisfies the Gibbs-Duhem criteria.³⁰ While this new Maxwell-Stefan framework

addresses the Gibbs-Duhem failure and satisfies the Onsager reciprocity relationship, it does require estimates of molar volumes within the membrane phase. This new "extended" framework assumes no volume change upon mixing and splits the polymer into "segments" where each segment is said to have the same molar volume as the solvent penetrant. Ribeiro, Freeman, and Paul derived an updated framework based on a volume fraction approach but removed the need for an arbitrary reference volume when determining the Maxwell-Stefan diffusion coefficients. ³¹ This updated form retains the benefits of the volume fraction system originally adopted by Heintz and Stephan.

Krishna developed a linearized set of Maxwell-Stefan equations from the updated framework laid out by Ribeiro et al., shown in equation 3-5.³² With certain assumptions, this allows for the solution of these Maxwell-Stefan equations without solving multiple ODEs. This matrix form of the Maxwell-Stefan framework for two penetrants is used in this work to model solvent transport through the polymeric phase:

$$\begin{pmatrix} N_1^V \\ N_2^V \end{pmatrix} = -\begin{bmatrix} B_{11} & B_{12} \\ B_{21} & B_{22} \end{bmatrix}^{-1} \begin{bmatrix} \Gamma_{11} & \Gamma_{12} \\ \Gamma_{21} & \Gamma_{22} \end{bmatrix} \begin{pmatrix} \frac{d\phi_1}{dz} \\ \frac{d\phi_2}{dz} \end{pmatrix}$$
(3)

$$B_{11} = \frac{\phi_2}{\theta_{12}^V} + \frac{\phi_m}{\theta_{1m}^V}; \quad B_{12} = -\frac{\phi_1}{\theta_{12}^V}$$
 (4)

$$B_{21} = -\frac{\phi_2}{\Theta_{21}^V}; \quad B_{22} = \frac{\phi_1}{\Theta_{21}^V} + \frac{\phi_m}{\Theta_{2m}^V}$$

$$\Gamma_{ij} = \frac{\phi_i}{\phi_j} \frac{\partial \ln a_i}{\partial \ln \phi_j}; i, j = 1, 2 \tag{5}$$

where N_i^V is the volumetric flux of component i, ϕ_i is the volume fraction of component i, Θ_{ij}^V is the modified Maxwell-Stefan diffusivity for the solvent pair, $\Theta_{i,m}^V$ is the Maxwell-Stefan diffusivity, which reflects the influence of the membrane on the penetrant, z is the distance into the membrane, and a_i is the activity of component i.

The D_{ij} terms are referred to as exchange coefficients and represent the coupling effects between two species. These coupling effects are akin to the species exerting drag on one another, resulting in a slowing down of the fast species and faster transport of the slow species. As the exchange coefficient increases in value, coupling effects decrease. A logarithmic interpolation, known as the Vignes correlation and shown below, has frequently been used to predict the exchange coefficients, where \overline{V}_i is the partial molar volume of species i.

$$\begin{pmatrix} \frac{\mathbf{D}_{12}^{\mathsf{V}}}{\overline{\mathbf{V}}_2} \end{pmatrix} = \begin{pmatrix} \frac{\mathbf{D}_{21}^{\mathsf{V}}}{\overline{\mathbf{V}}_1} \end{pmatrix} = \begin{pmatrix} \frac{\mathbf{D}_{1,m}^{\mathsf{V}}}{\overline{\mathbf{V}}_2} \end{pmatrix}^{\phi_1/(\phi_1 + \phi_2)} \begin{pmatrix} \frac{\mathbf{D}_{2,m}^{\mathsf{V}}}{\overline{\mathbf{V}}_1} \end{pmatrix}^{\phi_2/(\phi_1 + \phi_2)} \tag{6}$$

Some assumptions in the use of these Maxwell-Stefan equations for modeling permeation through glassy polymer materials are:

- The partial molar volume of each component is equivalent to its molar volume at pure conditions, 298 K, 1 atm
- The three-step sorption-diffusion mechanism applies (feed phase equilibrium, diffusion through active layer, and subsequent permeate phase equilibrium)
- No external mass transfer limitations (e.g., concentration polarization)
- No resistance to transport in the support layer
- Isothermal membrane layer
- Flory-Huggins type sorption behavior
- $D_{i,m}$ is independent of concentration

The boundary conditions for the glassy polymer framework are:

Feed side

$$z = 0;$$
 $\phi_i = \phi_i^{m,feed}$

• Permeate side
$$z = \ell;$$
 $\phi_i = \phi_i^{m,perm}$

Where the feed- and permeate-side volume fractions in the membrane are found through Flory-Huggins type phase equilibrium calculations. To simulate the transport for ORSO through an active glassy polymer membrane layer, the numerical method outlined in Mathias et al. was used, which takes a shooting algorithm approach. This splits the 2-point boundary value problem into an inner and outer solver. The inner solver integrates across the membrane layer while the outer solver takes the final integrator value and converges the permeate phase compositions and total flux through the active membrane layer (see Figure S4 for simplified flowchart). For a more indepth description of how the Maxwell-Stefan framework used in this work for polymers operates (numerical methods, boundary conditions, etc.) the authors would like to direct the reader to recent work by Mathias et al.³³

To fit Maxwell-Stefan diffusivities based on pure component fluxes, this modeling and simulation framework (Figure S4) is used for n = 1. Using our code for single component permeation simulations, a single variate solver was used to iterate across different diffusivity values. This was done until the simulated flux matched the experimental flux at a given system temperature, feed pressure, permeate pressure, and sorption parameters for Matrimid®.

3.2 Rigid Microporous Transport

Microporous (especially ultramicroporous) rigid inorganic fillers also abide by the sorptiondiffusion method of guest permeation. The rigidity of these fillers, as opposed to non-equilibrium glassy polymeric matrices, simplifies the observed sorption and diffusion processes to some degree.

As with polymers, the Maxwell-Stefan methodology has proven an accurate method of modeling transport in zeolites, MOFs, and carbons. Multiple studies have applied and refined the Maxwell-Stefan expressions and how they apply to microporous fillers. A review of zeolite transport was conducted by Keil, Krishna, and Coppens, with a substantial focus on Maxwell-Stefan transport. Maxwell-Stefan transport.

The Maxwell-Stefan equation for a zeolite (and other rigid microporous materials) has been described by Krishna and Baur.³⁷

$$-\rho \frac{\theta_i}{RT} \frac{\partial \mu_i}{\partial z} = \sum_{\substack{j=1\\j\neq i}}^n \frac{q_j N_i - q_i N_j}{q_{i,sat} q_{j,sat} \theta_{ij}} + \frac{N_i}{q_{i,sat} \theta_{i,m}}, i = 1, 2, \dots, n$$

$$(7)$$

With z representing the depth of the membrane, fractional occupancies are defined as

$$\theta_i = \frac{q_i}{q_{i,sat}} \tag{8}$$

with q_i being the molar loading of species i and the saturation loading being $q_{i,sat}$. In the case of zeolites, carbon molecular sieves, and other rigid microporous materials, the effect of the framework on the penetrating species is reflected in $D_{i,m}$, or the single component Maxwell-Stefan diffusivities. These values can be determined by applying a thermodynamic correction to recorded Fickian diffusivities. For these microporous materials this takes the form of 36

$$D_{i,m} \equiv \mathcal{D}_{i,m} \frac{\mathrm{d} \ln f_i^m}{\mathrm{d} \ln \theta_i^m} = \mathcal{D}_{i,m} \frac{\mathrm{d} \ln f_i^{fl}}{\mathrm{d} \ln \theta_i^m} \tag{9}$$

with f_i^{fl} being the fugacity of component i in the fluid phase and θ_i^m that components fractional occupancy in the membrane. Equation 9 successfully removes the effect of sorption from the transport diffusivity, and in the case of simple Langmuir sorption can be simplified to

$$\Theta_{i,m} = D_{i,m}(1 - \theta_i^m) \tag{10}$$

In this work, we describe sorption in the filler phase using the Langmuir model as this accurately describes the penetrants of interest's sorption with our materials. If the sorption of a component does not follow the Langmuir sorption model, it would be necessary to start again at equation 9 and derive the appropriate thermodynamic correction.

Lastly, equation 7 can be reformed as a set of matrices ³⁶⁻³⁷

$$(\mathbf{N}) = -\frac{\rho}{\ell} [\mathbf{q}^{\text{sat}}] [\mathbf{B}]^{-1} \theta_V^m \frac{\partial (\mathbf{F})}{\partial n}$$
 (11)

Where ρ is the density of the microporous material, ℓ is the membrane thickness, η is a dimensionless position along the length of the membrane, \mathbf{F} is a dimensionless fugacity where $F_i = b_i \hat{f}_i$ with b_i being the Langmuir affinity constant, \mathbf{N} is a matrix of the molar fluxes, and $[\mathbf{q_{sat}}]$ is a diagonal matrix of the saturation loadings. The components of the diffusion matrix, $[\mathbf{B}]$, are

$$B_{ii} = \frac{1}{\theta_{i,m}} + \sum_{j=1, j \neq i}^{n} \frac{\theta_j^m}{\theta_{ij}} \text{ and } B_{ij} = -\frac{\theta_i^m}{\theta_{ij}}, i \neq j$$

$$\tag{12}$$

To calculate the exchange coefficients for the rigid microporous framework case, a Vignes correlation was again used:

$$\mathbf{D}_{ij} = \mathbf{D}_{ji} = \mathbf{D}_{i,m}^{\theta_i^m / \left(\theta_i^m + \theta_j^m\right)} \times \mathbf{D}_{j,m}^{\theta_j^m / \left(\theta_i^m + \theta_j^m\right)}$$
(13)

Some assumptions in the use of these Maxwell-Stefan equations for modeling of permeation through rigid microporous materials are:

- The three-step sorption-diffusion mechanism applies (feed phase equilibrium, diffusion through active layer, and subsequent permeate phase equilibrium)
- No external mass transfer limitations (e.g., concentration polarization)
- Isothermal membrane layer
- $D_{i,m}$ is independent of concentration
- Langmuir sorption of penetrants (supported experimentally)

The boundary conditions for the rigid microporous framework are:

• Feed side

$$z = 0;$$
 $\eta = 0;$ $f_i^{fl,feed} = f_i^{m,feed}$

Permeate side

Permeate side
$$z = \ell;$$
 $\eta = 1;$ $f_i^{fl,perm} = f_i^{m,perm}$

While this is a brief overview of the Maxwell-Stefan formulations for organic solvent flux through rigid microporous materials, a more detailed account of these formulations can be found in the work of Ma et al along with Krishna and Baur. 36-37

3.3 Mixed Matrix Membrane Transport

Mixed matrix membranes are composite systems, and the preceding models provide frameworks for predicting the flux through both continuous and filler phases (the flux predicted through the filler phase assumes an all-filler membrane, which enables estimates of filler permeabilities). There are multiple models that seek to combine the polymer and filler properties to predict MMM transport, including those taking the resistance model approach, which models the MMM as an analogue to an array of resistors. 38-39 The Maxwell model, equation 14, has seen widespread use and assumes a random distribution of particles that do not interact with each other, resulting in the following equation:⁴⁰

$$\mathbb{P}_{MMM} = \mathbb{P}_{C} \left[\frac{\mathbb{P}_{D} + 2\mathbb{P}_{C} - 2\phi_{D}(\mathbb{P}_{C} - \mathbb{P}_{D})}{\mathbb{P}_{D} - 2\mathbb{P}_{C} + \phi_{D}(\mathbb{P}_{C} - \mathbb{P}_{D})} \right]$$
(14)

with \mathbb{P} representing the stated phase's permeability, where MMM, D, and C subscripts refer to the mixed matrix membrane, dispersed phase (filler), and the continuous phase (polymer), respectively, and ϕ_D is the volume fraction of the dispersed phase.

While the Maxwell model has seen extensive use, it has a well-known drawback in regards to volume loading. The Maxwell model relies on the assumption that inter-particle interactions between the randomly distributed filler particles are absent. While this assumption is valid at low volume fractions, it breaks down as the volume loading increases (generally >30%), and cannot account for the percolation phenomena. In this work, we focus on the dilute filler regime, which is aligned with the core assumptions of the Maxwell model.

An inherent risk in the formation of MMMs is the possibility of non-ideal interfacial phenomena occurring between the filler and polymer. Moore and Koros review a range of possible interfacial phenomena and how they affect membrane performance. 41 A common interfacial defect results from poor adhesion between the filler and polymer, creating a gap between the two. These defects can range in size from single angstroms to tens of nanometers and are often referred to as a sievein-a-cage defect and are a common cause of poor selectivity in MMMs. Depending on the size of the defect and the nature of the penetrant, transport in this defect can take on different forms, but all are a departure from the solution-diffusion regime that governs ideal MMM transport. For gases, the length scale of these defects places guest transport in the Knudsen regime. Mahajan and Koros describe this situation and demonstrate how a varied defect size changes the membrane's separation properties. 42 In the case of solvents, a liquid develops within the interface, allowing for the components to diffuse through the liquid and bypass the filler; it is unclear if Poiseuille flow mechanisms are important in these interfacial defects. Mahajan and Koros account for interfacial defects through a 3-phase modified Maxwell model. First, they combine the permeabilities of the defect and filler using the Maxwell model, and this combined permeability is used with the polymer permeability to calculate the MMM permeability, again using the Maxwell model.

Felske developed a model to address these interfacial nonidealities using an effective medium approach similar to Maxwell.⁴³ The Felske model approaches the matrix, interfacial region, and filler as a core-shell model with the matrix and interfacial region represented by the shells. Like the Maxwell model, the Felske model's predictions fail as the volume loading increases. However, the model (shown in equations 15-17) is simpler than the modified Maxwell model.

$$\mathbb{P}_{MMM} = \mathbb{P}_{C} \left[\frac{2(1-\phi) + (1-2\phi)(\beta/\gamma)}{(2+\phi) + (1-\phi)(\beta/\gamma)} \right]$$
 (15)

$$\beta = (2 + \delta^3)\lambda_{dc} - 2(1 + \delta^3)\lambda_{Ic} \tag{16}$$

$$\gamma = (1 + \delta^3) - (1 - \delta^3)\lambda_{dI} \tag{17}$$

In the case of the Felske model, ϕ is the volume fraction of the core-shell particles, δ is the ratio of the outer interfacial radius to the inner core radius, and λ_{ij} is the permeability ratio of *i* over *j*, where the subscripts d, I, c corresponds to the permeabilities of the filler, interface, and continuous

layer respectively. It becomes apparent that as the interfacial region disappears ($\delta \to 1$), the equation becomes the Maxwell model shown in equation 14. These models and others are reviewed in depth in multiple literature sources.^{39, 44-45}

While these models are valuable tools in analyzing non-ideal interfaces present in many MMMs, this paper's modeling work focuses on polymer/filler property matching and not on the effect of non-ideal phenomena (interfacial voids polymer rigidification, percolation, etc.). The original Maxwell model in equation 14 has been used to describe guest transport within these types of idealized MMMs with good success and is a useful starting point before considering additional complexities. Interfacial issues in mixed matrix OSRO membranes are largely unexplored and are a ripe area for future research

A particular challenge addressed here is the combination of the Maxwell model (based in permeabilities) and the Maxwell-Stefan models, which report component fluxes in liquid phase systems. A key challenge is that the permeability, shown in equation 18, is poorly defined in OSRO compared to gas separation cases. For a pure component permeation, the permeability can be reasonably defined as:

$$\mathbb{P} = \frac{N\ell}{\Delta f} \tag{18}$$

Where ℓ is the membrane thickness and Δf is the transmembrane fugacity. However, due to the strongly coupled nature of the driving forces in liquid permeation, this expression of permeability is only approximately applicable in nearly pure solvents. Support for this assumption is shown through analysis of Onsager's theory, where the flux of component i in a multicomponent mixture can be represented through⁴⁶⁻⁴⁹

$$N_i = \sum_{j=1}^n L_{ij} \operatorname{RTVln}(f_j) \tag{19}$$

where L_{ij} is a phenomenological constant. In the case of diffusion, equation 19 can be represented as

$$N_i = \sum_{j=1}^n \frac{\mathbf{D}_{ij} C_j^m \nabla f_j}{f_i} \tag{20}$$

Inserting equation 20 into 18, assuming a binary mixture, yields

$$\mathbb{P}_{1} = \frac{\left(\frac{\mathbb{P}_{11} c_{1}^{m} \nabla f_{1}}{f_{1}} + \frac{\mathbb{P}_{12} c_{2}^{m} \nabla f_{2}}{f_{2}}\right) \ell}{\Delta f_{1}} \tag{21}$$

Equation 21 shows that the coupled driving forces can only be ignored for sufficiently dilute systems or for very weak coupling of guest species such that equation 18 is approximately correct.

To address this complicating factor, we have chosen to define the performance of our materials when challenged with pervaporative separations. The pervaporation permeabilities are used to define filler properties and were not used in any OSRO output calculations. We use these pervaporation-based properties because the permeability of an OSRO system is poorly defined, as

shown in equation 21. Additionally, perm-selectivity (i.e., $\mathbb{P}_i/\mathbb{P}_j$) cannot be defined due to the downstream conditions in OSRO. Permeability and perm-selectivity are nevertheless valuable descriptors for membrane materials as these are linked to the diffusion and sorption characteristics of the materials, with the perm-selectivity being reflective of the intrinsic separation performance of the filler. To highlight how these pervaporative permeabilities are used in our model, a simplified flow sheet outlining the OSRO model and its outputs is presented in Figure 1. For each of the three membranes (polymer, filler, MMM) the model outputs a separation factor (β), shown in equation 22, and a <u>normalized</u> OSRO permeability, described in Figure 2.

$$\beta_{1/2} = \left[\frac{C_1}{C_2} \right]_{permeate} / \left[\frac{C_1}{C_2} \right]_{feed}$$
(22)

Where C_i is the molar concentration of component i. These pervaporation permeabilities were normalized against the polymer's pervaporation permeability, as we are primarily concerned with the ratios of filler to polymer performance in this work. The elimination of downstream influences simplifies the description of filler properties and allows for perm-selectivites (α) of the fillers to be described as:

$$\alpha_{i,j} = \frac{\mathbb{P}_{i,filler}(\text{pervap})}{\mathbb{P}_{j,filler}(\text{pervap})}$$
(23)

A flowsheet describing the process of calculating the filler pervaporation properties is shown in Figure 2. While Figures 1 and 2 provide a high-level overview of how different pieces of the model fit together, a more detailed look into how the models operate is provided in Figures S4-6.

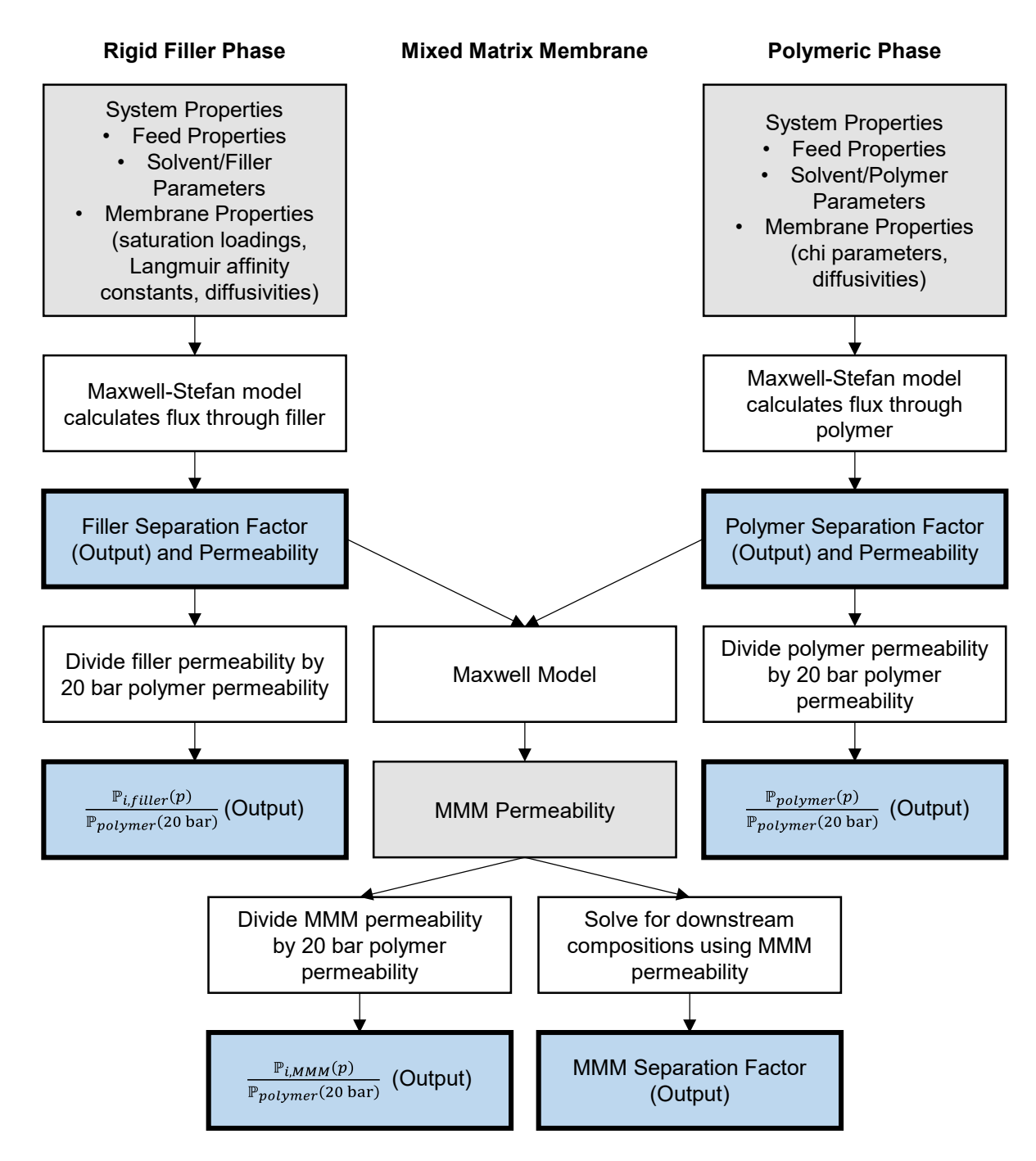


Figure 1: Simplified flowsheet detailing the models used to determine separation factors and permeabilities for the polymer, filler, and MMM. Note that all output permeabilities are normalized to the polymer's permeability at 20 bar.

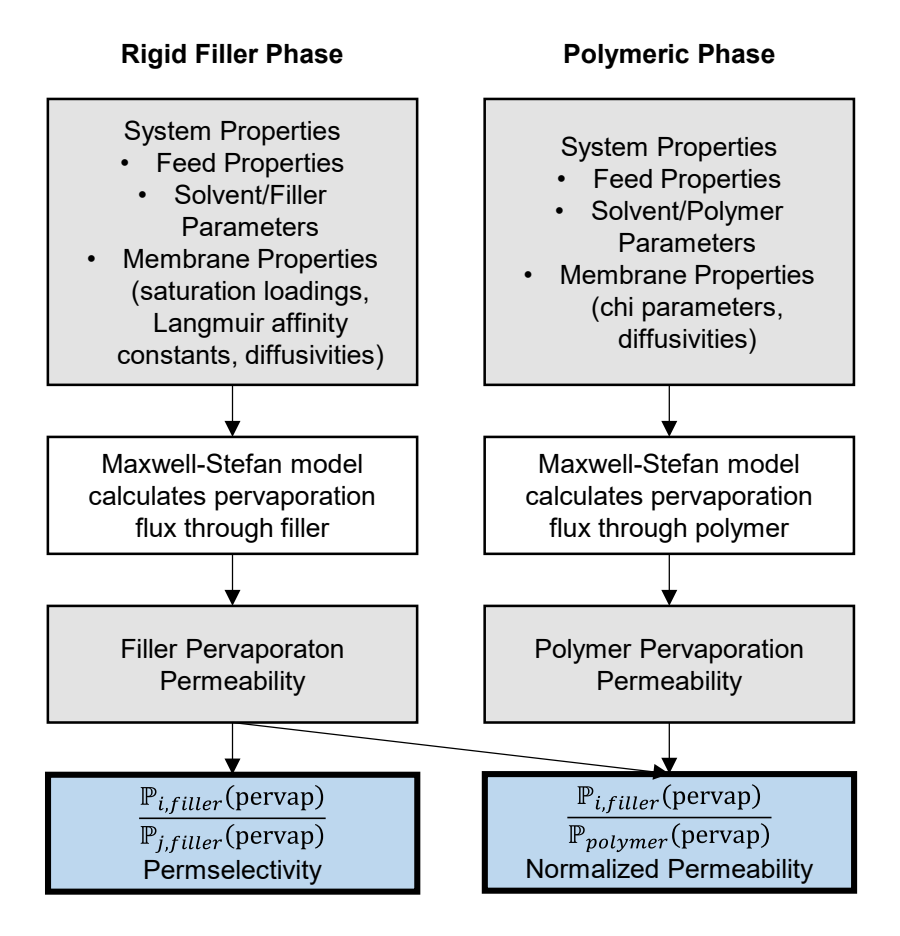


Figure 2: Simplified flowsheet detailing the method of determining pervaporation benchmarked filler characteristics. The use of pervaporation for these descriptive properties is useful as it removes the influence of a liquid downstream phase

4. Methods and Materials

4.1 Materials

Matrimid® 5218 was purchased from Huntsman Corporation, UiO-66 was purchased from Inmondo Tech, both were dried under vacuum overnight at 100 °C before use. Anhydrous n-methylpyrrolidone (NMP), ethanol (EtOH), tetrahydrofuran (THF), toluene, and mesitylene were all purchased from Sigma-AldrichTM. Methanol and hexane used in solvent exchanging were purchased from VWRTM. The p-xylylenediamine used for diamine cross-linking of Matrimid® was purchased from TCITM. Fiber modules were created using Swagelok® tubing and LOCTITE® EA E-60NC potting compound.

4.2 Materials Characterization

IR spectra of cross-linked and uncrosslinked membranes were collected with a Nicolet iS10 (Thermo Fisher, Waltham, MA). SEM micrographs were captured on a SU8230 (Hitachi, Tokyo, Japan). N₂ physisorption was conducted using a Quadrasorp Evo (Quantachrom, Boynton Beach,

FL). Thermogravimetric analysis of UiO-66 was conducted under air using a TGA Q500 (TA Instruments, New Castle, DE). Characterization of these materials can be found in the supplementary information. N₂ physisorption was carried out using a Belsorp max (BEL Japan Inc., Osaka, Japan).

4.2 Hollow Fiber Dope Preparation

Two dopes were created for the dual-layer spinning process: core and sheath. The core dope is responsible for the majority of the fiber mass and creates its porous substructure; UiO-66 is absent from this dope. The necessary ratios of dry polymer, anhydrous solvents, and non-solvents (table 1) were added together in a 1 L glass jar. The jar was sealed and placed on a roller to homogenize, which typically required a few days. Prior to spinning, the dope was loaded into a 1000D high-pressure syringe pump (Teledyne Isco, Lincoln, NE) and allowed to degas for at least 24 hr. at 50 °C to remove trapped air.

The sheath dope comprises the outside of the hollow fiber and creates the selective layer. Thus, the UiO-66 need only be present in this layer. The sheath dope fabrication process was adapted from work presented in Zhang et al.²¹ First, a prime dope was created using 20% of the total required liquids and polymer. These were mixed in a glass jar, sealed, and placed on the roller to dissolve and homogenize. A dispersion dope was created using 80% of the NMP and all of the UiO-66. The exclusion of the volatile components at this stage aims to reduce mass loss due to evaporation during dope preparation. The dispersion dope was rotated between sonication (Branson Digital Sonifier, Branson Ultrasonics, Danbury, CT) and a shear mixer multiple times. After sufficient dispersion of UiO-66 was achieved, the dispersion dope was placed on the shear mixer and the remaining volatiles were added, immediately followed by the prime dope. The prime dope increases the viscosity of the solution, greatly reducing the propensity of UiO-66 to settle. After the mixture was homogenized by the shear mixer, it was subjected to repeated sonication and mixing as described earlier. The mixture was kept in an ice bath throughout the process to suppress temperature increases due to sonication. After the final round of sonication, the dope was placed on the shear mixer and heated to 50°C. The remaining Matrimid® was slowly added to the stirred solution. After the addition of all remaining polymer, the dope was impelled for at least three hours under heat to fully dissolve the polymer in the dope. Once the dope was observed to be homogenous, it was removed from the shear mixer and heat, capped, sealed, and placed on the roller to ensure full dissolution and dispersion. Before spinning, the dope was poured into a 1000D high-pressure syringe pump (Teledyne Isco, Lincoln, NE) and allowed to degas at 50°C for at least 24 hrs.

Table 1 lists the dope compositions for the selected volume fractions of the UiO-66 within the fiber. The concentration of ethanol in the sheath dope was decreased relative to the core dope to help create defect-free skin layers. The MMMs were spun using the core and sheath dope listed, while the pure Matrimid® membrane used a single dope.

Table 1: The dope compositions for the spun hollow fiber membranes. The sheath & core composition corresponds to the 10 vol% MMM, while Matrimid® is for pure Matrimid® membranes

| Dope Compositions (wt %) | | | | |
|--------------------------|-------|--------|-----------|--|
| | Core | Sheath | | |
| | 0 wt% | 10 wt% | Matrimid® | |
| Matrimid | 26.2 | 25.0 | 26.2 | |
| UiO-66 | | 2.8 | ı | |
| NMP | 51.3 | 48.0 | 53.0 | |
| THF | 5.7 | 12.0 | 5.9 | |
| EtOH | 16.8 | 12.2 | 14.9 | |

4.3 Hollow Fiber Spinning

Fabrication of dual-layer hollow fibers utilized a dry-jet wet-quench setup. ^{21, 50} The sheath and core dopes are coextruded with an NMP/Water (92/8 for 10 vol%, and 95/5 for pure Matrimid) bore fluid through an annular spinneret, into an air gap, before submersion in a non-solvent water quench bath where rapid phase inversion of the fiber occurs. The phase inverted fibers exit the quench bath, where they are collected on a rolling drum in a separate water bath. The fibers are left on this drum for at least 10 min to ensure full phase inversion before removal to a separate bath of deionized water. This separate DI water bath is replaced every day for three days and ensures the full removal of solvent molecules within the fiber. After these water exchanges, the fibers are washed in methanol three times for 20 min, followed by three more 20-minute washes in hexane. After the final hexane wash, the fibers are hung in ambient conditions for an hour to dry before being placed in a 60°C vacuum oven (-29 in Hg) overnight.

Membranes can only tolerate a small number of skin layer defects, as defects can quickly eliminate membrane selectivity for small organic solvent molecules.⁵¹ It is critical to properly balance multiple spinning variables with the dope composition to fabricate high-quality hollow fibers. The spinning parameters used to create the hollow fibers in this work are shown in table 2. The quench bath temperature and the air gap were some of the more impactful parameters in creating high-quality fibers for this dual-layer spin. The quench bath temperature strongly influences solvent diffusion and thus the rate of phase inversion for extruded fibers. The air gap has a direct relationship with the skin layer thickness, as the formation of the dense skin layer is driven primarily by the evaporation of volatile components during fiber residence in the air gap.

Table 2: Spinning parameter ranges for the fabrication of UiO-66/Matrimid hollow fiber membranes

| | Matrimid ® | 10 vol% UiO-66 |
|---------------------|------------|----------------|
| Air Gap (cm) | 8.0 | 9.5 |
| Bore Flow (mL/hr) | 100 | 60 |
| Core Flow (mL/hr) | 360 | 160 |
| Sheath Flow (mL/hr) | - | 40 |
| Take Up (m/min) | 40 | 38 |
| Dope Temp (°C) | 50 | 50 |
| Bath Temp (°C) | 25 | 20 |

4.4 Crosslinking of Spun Hollow Fibers

A diamine crosslinker was utilized to react with imide rings along the Matrimid® backbone. The diamine cross-linking of the Matrimid® has been adapted from previous works. ^{10, 52-54} Briefly, 0.05 g/mL of p-xylylenediamine was dissolved in methanol. The hollow fibers were submerged in this solution for one hour at room temperature before being rinsed in fresh methanol three times for 20 minutes each to remove any unreacted crosslinker. The fibers were left to air dry overnight before being placed in a vacuum oven at 60°C to remove any residual solvent.

4.5 Binary Organic Solvent Reverse Osmosis Separation

A mixture of 98/2 mole % toluene/mesitylene was used to evaluate the solvent separation performance of the cross-linked fibers. The combination of toluene (92.14 g/mol) and mesitylene (120.19 g/mol) is an aromatic mixture with only a slight difference in size; this provides an excellent choice in evaluating the size-selective capabilities of membranes in an OSRO regime.

Two 500D syringe pumps (Teledyne Isco, Lincoln, NE) with a continuous flow electronic valve package provided constant pressure over multi-day runs. Figure 3A lays out the general testing setup, with the module receiving a pressurized feed from the pump before the retentate and permeate were recycled into the feed solution. A needle valve on the retentate maintained the pressure and adjusted the flowrate to ensure low stage cuts, i.e., <5%.

Prior to pressurization, the feed solution was slowly passed through both the shell and bore sides of the module overnight to prewet and remove air bubbles that could possibly damage the membrane. After this prewetting, one end of the bore was capped and the other connected to a tube leading back to a solvent reservoir. As mentioned earlier, the retentate flow rate was controlled using a needle valve such that the stage cut across the membrane was below 5%. The needle valve was closed during initial pressurization. Pressurization was done slowly (<10 psi/min) to avoid any damage or fiber collapse. Once the target pressure was reached the needle valve was slowly opened to allow retentate flow without dropping the pressure. This valve was left open for the remainder of the experiment regardless of pressure changes.

To ensure steady state, feed and permeate samples were collected over multiple days. The composition of these samples was determined using an AgilentTM 7890B GC, allowing for calculating the fiber's separation factor.

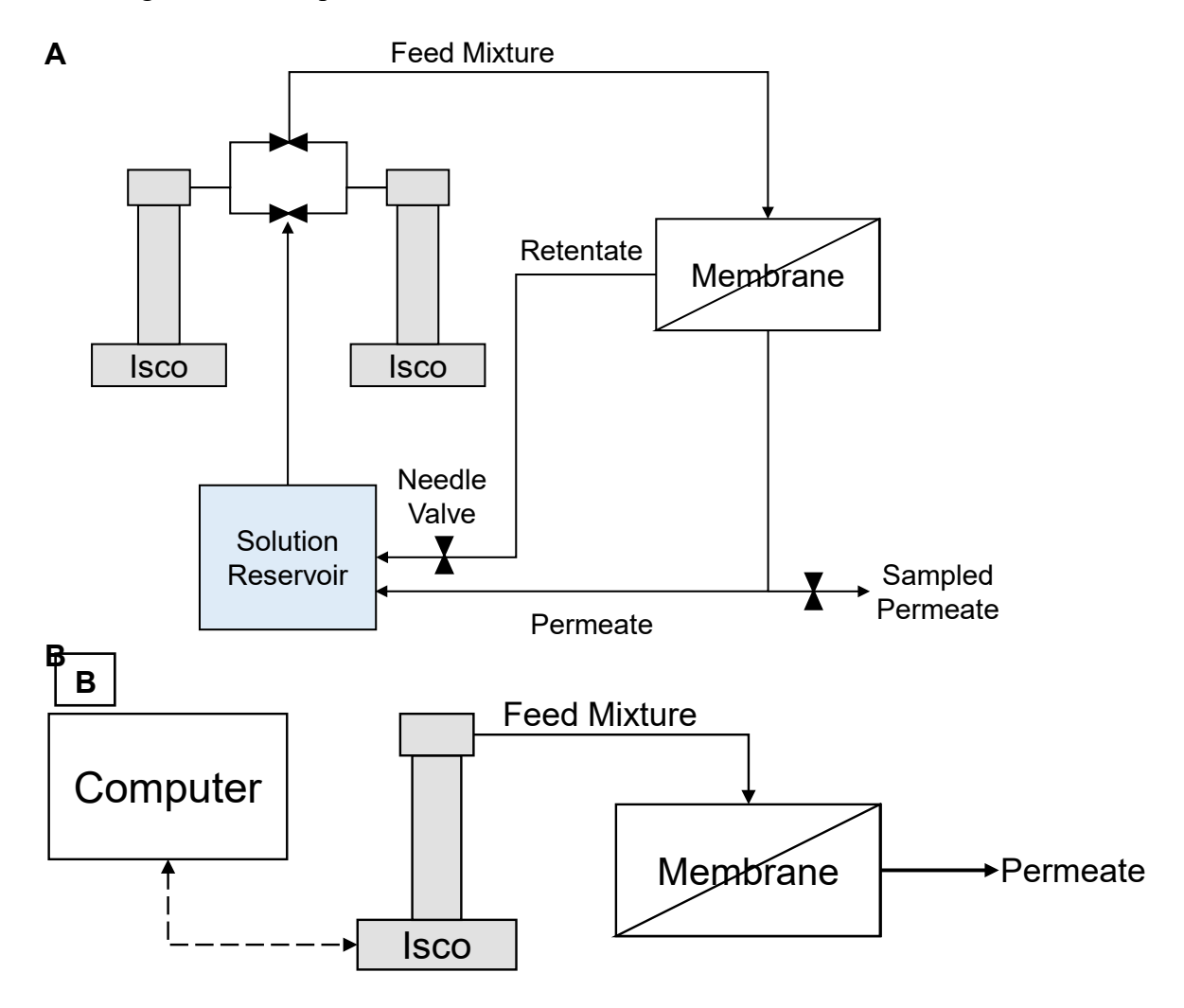


Figure 3: A) Dual Isco pump system configured for constant flow/pressure to module. The setup uses a Teledyne Isco™ pulseless valve setup to elimate pressure variations during pumps switch overs. A needle valve restricted retentate flow rate to elevate pressure in the module, and when permeate was not being collected for analysis, it was recycled into the reservoir B) Single pump setup for dead end pure component permeation. System utilizes a Teledyne Isco™ 500D pump connected to computer for data collection

4.6 Single Component Permeation

Dead end permeation was conducted on both the pure Matrimid® and 10% UiO-66/Matrimid® membranes. The pure component permeation enables the calculation of guest diffusivity through the polymer membrane.

A single 500D syringe pump (Teledyne Isco, Lincoln, NE) was used for the pure component permeation experiments. Figure 3B lays out the general experimental setup for the dead-end system. The feed into the module is pressurized from the syringe pump upstream, and the permeate is collected. The pump is connected to a computer that records the syringe pump's volume change. This volume change data is used to calculate the flux of solvent through the membrane.

Prior to pressurization, the solvent was passed through the shell side of the module to remove any air pockets. Then the solvent was slowly passed through the bore side of the membrane to prewet the permeate side. Once all air bubbles were removed, and solvent had been passed through the bore, the pressure was slowly increased for the system. The pressure ramp was kept at a rate less than 10 psi/min to prevent any collapse or damage to the fiber. Data collection was then started on the computer. Steady state was ensured by monitoring the rate of volume change on the data collected on the computer. This data was double-checked against manually collected permeate samples.

4.7 Gravimetric Sorption

Gravimetric sorption of organic solvents was carried out using a TA VTI-SA+ (TA Instruments, New Castle, DE). A 1,000 min drying step at 120°C was carried out in situ prior to a run. To achieve different relative pressures of organic vapor, a vapor-loaded nitrogen stream was mixed with a dry nitrogen stream, with mass flow controllers regulating each stream to achieve the proper ratio. The resultant isotherms were then fitted to the Langmuir isotherm to determine the Langmuir affinity constant and saturation loading.

4.8 Unit Activity Polymer Swelling

Unit activity swelling of polymer samples provides a simple method for estimating the chi parameters used in the Flory-Huggins sorption model. In this work, dense cross-linked Matrimid® films were swollen using the solvents of interest: toluene and mesitylene. The cross-linked coupons were dried overnight at 80°C under vacuum to remove any residual water in the polymer matrix. The coupons were then submerged in solvent and left for over a month to reach equilibrium. When measuring, the exterior of the films were wiped dry to remove excess solvent. At least four coupons were measured for each film.

5. Results and Discussion

i. Characterization of membrane transport

Pure component transport studies provide a quick method in evaluating the potential of materials for a separation. The information from these studies is of particular interest to this work as it provides the diffusivities necessary for the polymer Maxwell-Stefan transport frameworks, which ultimately allows us to model how a MMM performs in multicomponent separations. The permeance of toluene and mesitylene in cross-linked hollow fiber Matrimid membranes is shown in Figure 4A.

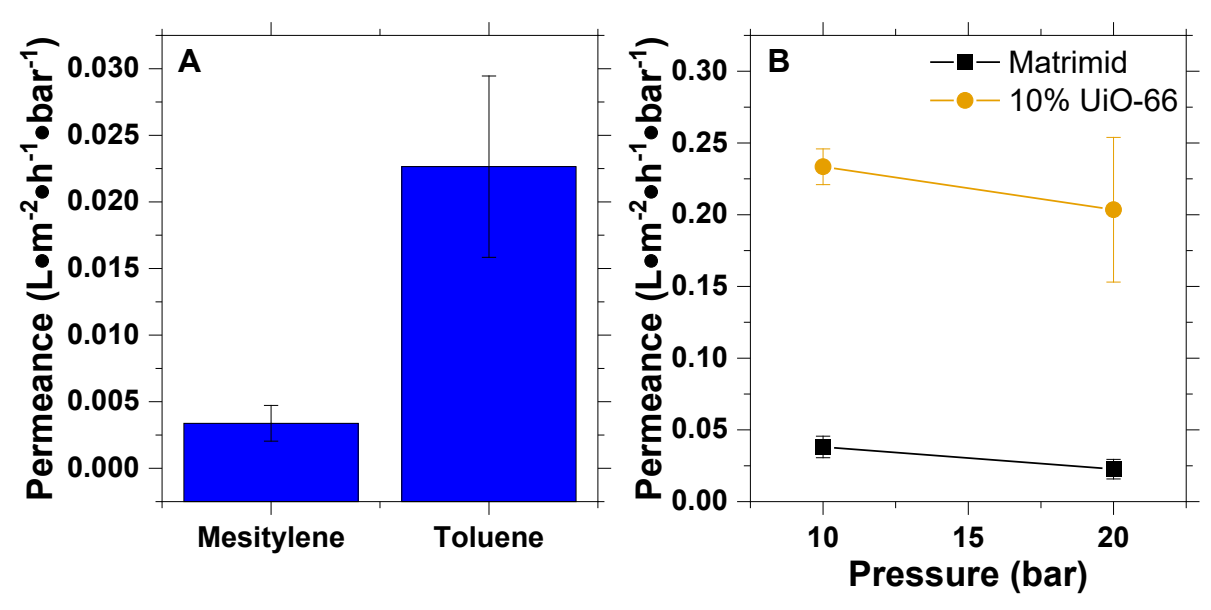


Figure 4: A) Solvent permeances across a crosslinked hollow fiber Matrimid® membrane with a transmembrane pressure of 20 bar B) Toluene permeances for Matrimid® and 10% UiO-66/Matrimid® membranes from 10 bar to 20 bar

These membranes are observed to have low permeances (approximately 0.02 and 0.003 L•m⁻¹•h⁻¹•bar⁻¹ for toluene and mesitylene, respectively). These low permeances are attributable to the post-fabrication cross-linking conducted on the Matrimid®. The diamine cross-linking rigidifies the polymeric matrix, reducing swelling and plasticization. This can potentially boost the selectivity of the membrane as well.

Figure 4B demonstrates the effect of UiO-66 upon the membrane permeance across two pressures. The inclusion of UiO-66 increases the membrane permeance by \sim 6x at 10 bar, with this growing to \sim 10x at 20 bar. This large difference in permeances points to the presence of UiO-66 as the primary factor. The porous UiO-66 provides for faster transport of toluene compared to the non-porous cross-linked Matrimid®, and thus increases the permeance of the MMM relative to the pure polymer.

ii. Characterization of MOF sorption properties

The filler sorption and diffusion properties are key inputs into our MMM transport model. Due to the difficulty in accurately measuring solvent diffusivities within these nanoscopic microporous materials, we do not attempt to measure the diffusivities. Instead, we vary the filler diffusivity within the model, which has the effect of changing the permeability of the MMM filler. This ultimately allows us to scan a range of filler permeabilities to match with a range of polymer permeabilities. Isotherms for toluene and mesitylene were measured using gravimetric sorption. Figure 5 displays the isotherms for each solvent along with the fitted Langmuir model.

$$q(f_i^{fl}) = q_i^{sat} \left(\frac{b_i f_i^{fl}}{1 + b_i f_i^{fl}}\right) \tag{24}$$

The Langmuir model, shown in equation 24 where b_i is the Langmuir affinity constant, provides a good fit to both isotherms, supporting the use of the Langmuir model derivation of equation 9.

The total pore volume and molar volumes of toluene and mesitylene were used to calculate the saturation loadings of each solvent in UiO-66. The total pore volume was calculated from N_2 physisorption data at a $P/P_0 = 0.65$ (calculation can be found in the SI). Toluene demonstrated a saturation loading of 5.36 mmol ${}^{\bullet}g^{-1}$, surpassing the 4.06 mmol ${}^{\bullet}g^{-1}$ saturation loading found for mesitylene. The higher saturation loading of toluene is likely attributable to its smaller size, allowing for more toluene molecules to fit within the UiO-66 framework.

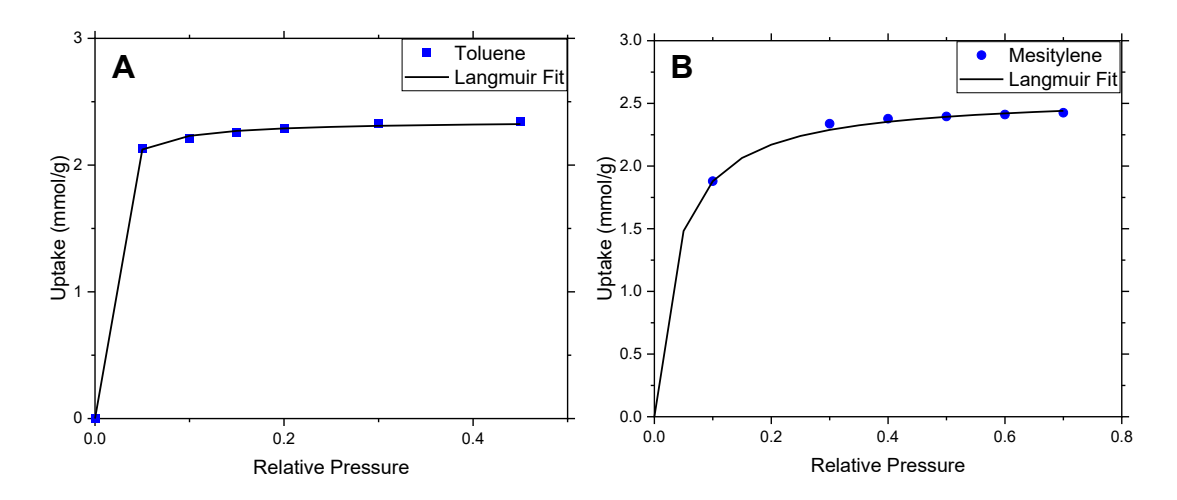


Figure 5: Vapor isotherms for UiO-66 for A) toluene and B) mesitylene, with the fitted Langmuir isotherm for each solvent

iii. Comparison of transport in polymers and MOFs

While mixed matrix membrane transport has been well documented and explored with gas separations, it is still relatively underdeveloped for solvent separations. Expanding our knowledge of this area will enable rapid screening of membrane materials, cutting down on costly experimental screening of material pairings, and ultimately accelerate the development of successful mixed matrix membranes. In addition, beyond identifying promising materials, this knowledge will help determine the cause of membrane issues in testing (e.g., interfacial defects).

Maxwell-Stefan models were developed for both the polymer and inorganic phase to account for the multicomponent nature of separations and combined with the Maxwell model to predict the MMM permeability. This combined model offers a facile method for the evaluation of membrane performance under different conditions. For this work, these models were used to describe a glassy polymer/rigid microporous filler MMM. This work aims to identify trends in membrane performance as a function of material properties and transmembrane pressure. The filler

permeability is described as the filler's pervaporation permeability normalized to the polymer's pervaporation permeability, while the perm-selectivity is the ratio of the filler's pervaporation permeability for two components, defined in equation 23. Pervaporation-based properties were chosen as the permeability and perm-selectivity can be defined precisely, unlike OSRO permeabilities. These pervaporation-based properties provide a simple way of describing the filler properties. The two separate OSRO models provide the predicted OSRO performance of both filler and polymer. Through the Maxwell model, the OSRO performance of these phases is used to predict the OSRO performance of the final MMM. The permeabilities of the theoretical filler are controlled by changing the guest diffusivity, while the sorption characteristics are set to those measured for UiO-66. The targeted separation for this model is a binary mixture of alkyl aromatics (e.g., toluene/mesitylene, *p*-xylene/*o*-xylene, etc.), which are an industrially important class of separations.⁵⁵

Figure 6 demonstrates how the solvent flux (toluene, in the current case) through an OSRO membrane changes as a function of the filler permeability and the feed pressure. The fluxes in these two figures are ratios, specifically the ratio of the material in question's flux to that of the base polymer; this normalization is chosen so that the results can be generalized to different polymer/filler systems. Figure 6A demonstrates how the flux of the solvent through the MMM and its constituent phases change as the permeability of the filler is increased in relation to the polymeric phase. As the permeability of the filler increases, one could expect to see a corresponding increase in the permeability of the MMM. Instead, we calculate that despite a coupling between the filler and MMM permeabilities at lower values, as the filler permeability continues to increase, the MMM permeability begins to plateau. This demonstrates that while the filler influences the permeability of the MMM, increases in filler permeability at a certain point begin to offer diminishing returns, which is consistent with observations in the gas separation literature. 40-41 As the permeability of the filler increases compared to the polymer, the transport through the polymer becomes rate-limiting. As the gap between the two permeabilities continues to increase, overall transport approaches an asymptote, as the filler effectively becomes a gap in the matrix relative to the polymer transport. Said more plainly, an infinite permeability applied in the filler reaches a finite permeability in the MMM, i.e., the polymer phase transport resistance dominates.

Figure 6B illustrates how the flux of the MMM and its constituent phases reacts as a function of pressure. It is well established that polymer membranes have an asymptotic response due to the occurrence of a finite driving force, and we see that this is in turn extended to the MMM. Interestingly, when preparing a MMM, we see that the response closely follows that of the polymer, not the filler, in terms of magnitude. This further reinforces the findings from Figure 6A that transport in the MMM is largely dominated by the polymeric phase.

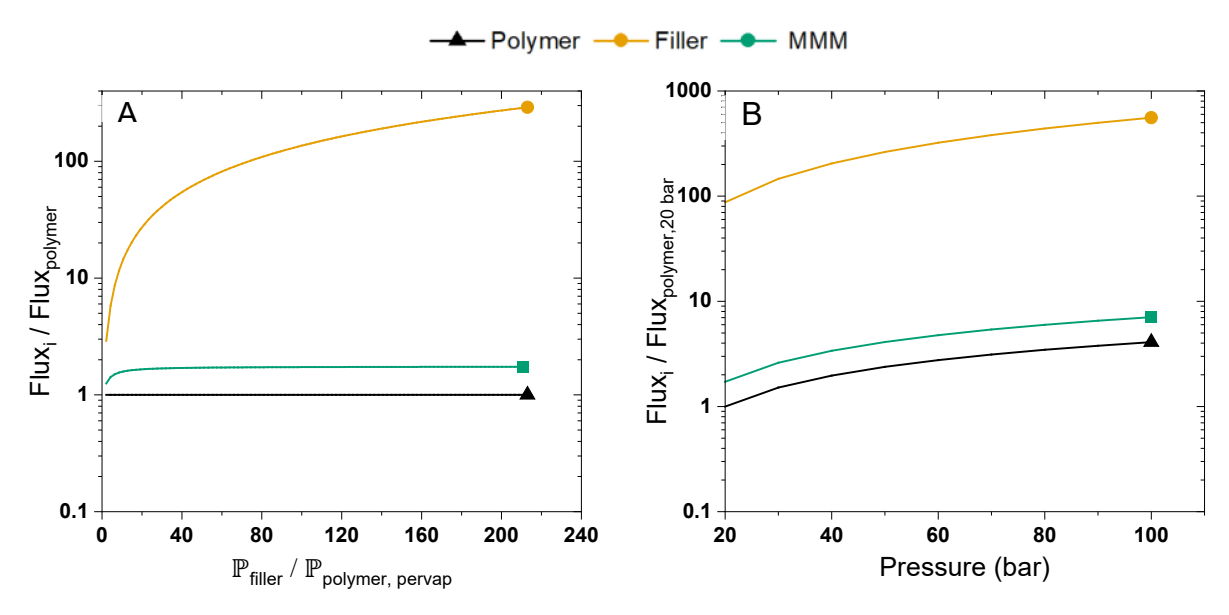


Figure 6: Model predictions. a) solvent fluxes of phase *i* (*where i refers to cases in the legend*) normalized to fluxes through polymer at 100 bar for the pure polymer, the MMM, and the filler. b) Solvent fluxes normalized to fluxes through pure polymer at 20 bar as a function of pressure. MMM calculations are for a 20 volume % MMM and its constituent phases. All modeled membranes have identical thicknesses, modelled fluxes are toluene.

Flux-pressure responses are useful first tests for any membrane material. However, the role of osmotic pressure is an additional complicating factor beyond those typically found in gas separations; moreover, there is a stronger effect of solvent-solvent coupling interactions relative to gas-gas pairs. Figure 7 highlights how membrane performance changes with pressure on a Robeson-style plot. Demonstrated here are the pressure responses for a cross-linked Matrimid® membrane, selective filler, and MMMs ranging from 10-50 volume % with pressures ranging from 20 bar to 100 bar. While the polymer membrane (cross-linked Matrimid®) has inherent selectivity for toluene over mesitylene, this selectivity is minimal in comparison to that of the filler. The MMMs benefit from the filler's performance and are predicted to demonstrate increasing permeance and selectivity as loading is increased. It is interesting to note that the pure filler is not expected to have dramatic changes in solvent permeance as a function of pressure, although major changes in separation factor are estimated. Despite these gains in permeability, the MMM performance is still much closer to that of the polymer rather than the filler, demonstrating that, similar to gas separations, the continuous phase of the MMM is the main determinant of a MMM's performance. Moreover, the base separation factor of the polymer largely controls the separation factor of the MMM; this indicates that while high loadings of selective fillers boost the MMM separation factor, a high-performance polymer is critical to achieving a MMM's potential fully. Indeed, our analysis shows that 50 vol% MMMs and 100 bar of transmembrane pressure yield only a ~4.5x increase in separation factor over the polymer, compared to a greater than 200x increase for the filler.

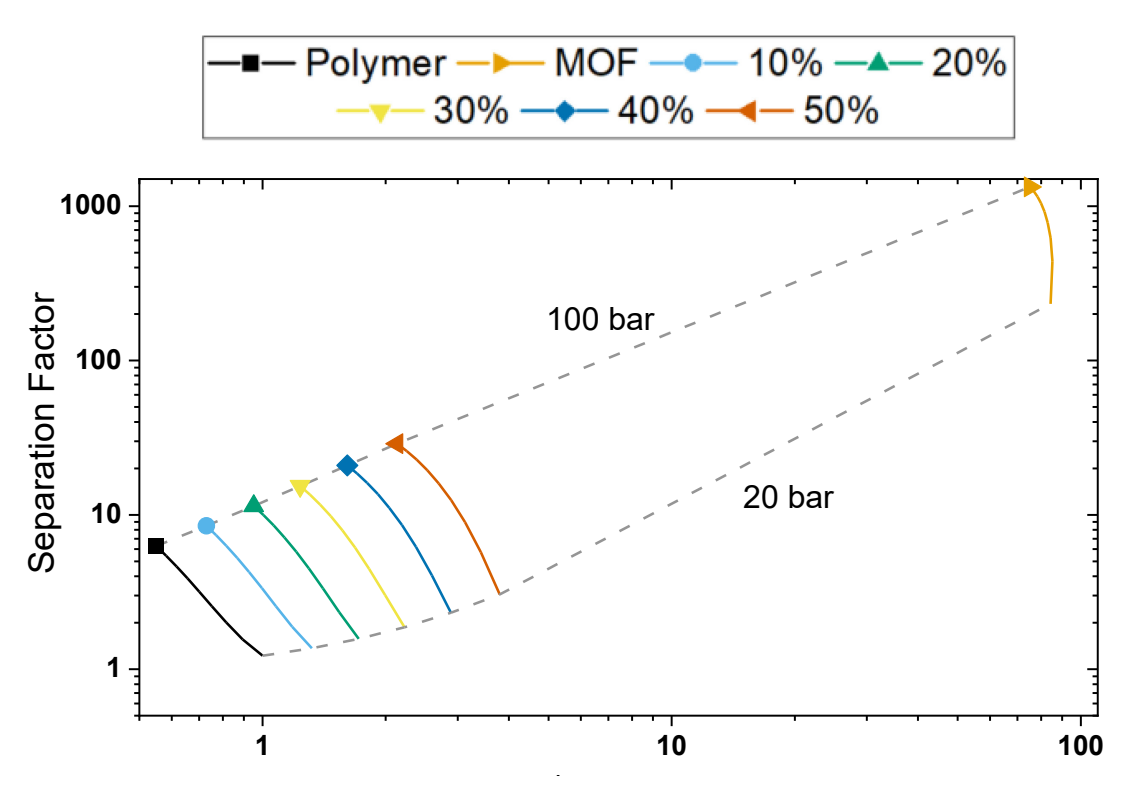


Figure 7: Modeled separation factors and permeabilities ratios for polymer, 10-50 vol % MMM, and MOF. The transmembrane pressure range for each membrane is from 20-100 bar. Permeabilities are normalized to the polymer's at 20 bar

iv. Polymer/Filler Matching

As a mixed matrix membrane is a composite system, the interplay of the two components' transport properties determines the final membrane performance. Understanding how these properties interact is crucial in "matching" a polymer with a suitable filler to optimize the resulting MMM performance. While choosing based on selectivity is fairly straightforward, i.e., a more selective filler will typically yield a more selective MMM, it has been shown in gas separations that the two materials' permeabilities play a large role in both the permeability and selectivity of the final membrane. This stems from the continuous polymer phase setting the baseline for permeability. If this baseline permeability is too high, the slower transport in the filler fails to boost the membrane's performance, while too low of a permeability restricts the amount of penetrant the filler interacts with, reducing potential gains in selectivity. While the importance of matching has not been explored in solvent separations, it stands to reason that proper matching will hold the same significance as it does in gas separation membranes.

Using the model outlined above, prospective fillers were evaluated with differing selectivity and permeance. This approach does not seek to target any specific filler or a singular solvent separation but instead looks to analyze broader trends that can inform polymer/filler matching across a wide range of solvent separations.

The responses to pressure of the polymer and four theoretical fillers of differing selectivities and permeabilities are shown in Figure 8A. For ease of visualization and comparison, all plotted permeabilities were normalized with respect to the polymer's OSRO permeability (Eq. 18) at a transmembrane pressure of 20 bar. As shown earlier, the polymer's permeability decreases as the pressure increases. We use the properties of cross-linked Matrimid® for these calculations. While both the polymer and filler demonstrate increases in separation factor as pressure is increased, the filler's increase outpaces that of the polymer. The larger increase in filler separation factor is due to the greater inherent selectivity of the filler particles, which is influenced by the well-defined pore size of the filler.

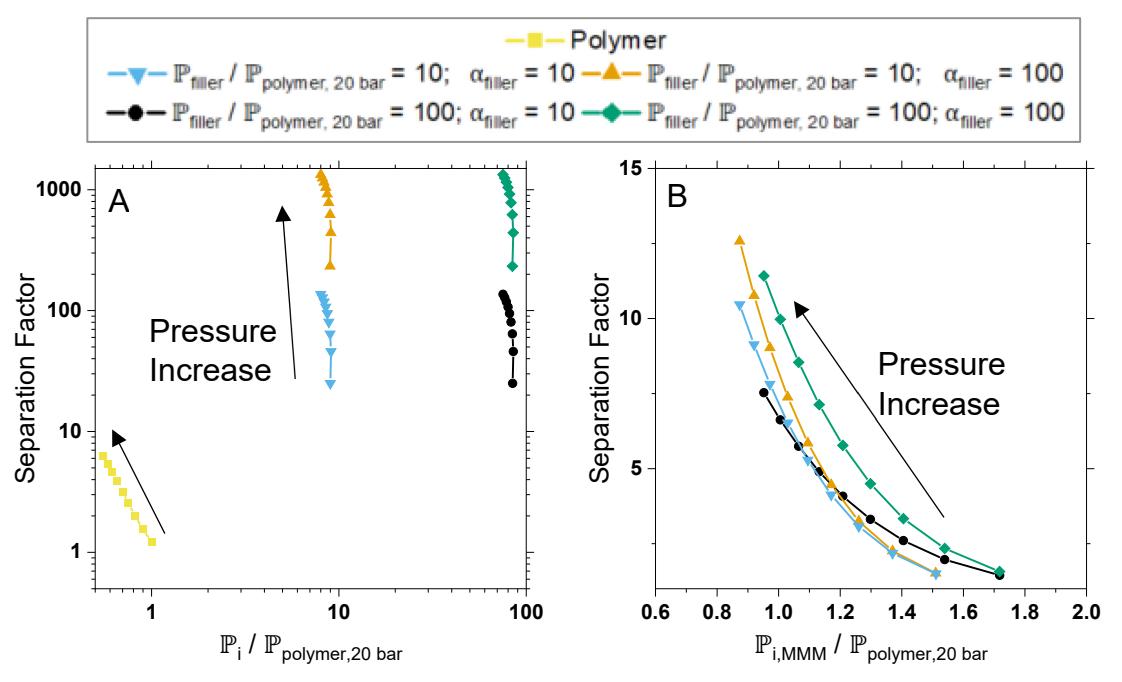


Figure 8: OSRO separation factor and normalized permeability as a function of pressure. A) Pressure responses for non-selective polymer and four theoretical fillers. The transmembrane pressure increases from 20 bar to 100 bar. B) Pressure responses for 20 vol% MMMs with four theoretical fillers. Each filler is described by the multiple of its pervaporation permeability over the polymer (P) and its permselectivity (α). Here, $\mathbb{P}_{i,MMM}$ refers to the OSRO permeability of the MMM. The transmembrane pressure increases ranges from 20 bar to 100 bar.

While the impact of the filler perm-selectivity (shown below) on the membrane's separation factor is clear, it does have a less clear role in the MMM's permeability. Importantly, as shown in Figure 8B, higher filler perm-selectivity leads to higher separation factors. Therefore, all else being the same, one would look for a filler with the maximum selectivity. While this relationship between filler perm-selectivity and separation factor is clear, we see that MMMs with identical perm-selectivities have different separation factors based on filler permeability. This shows that selection of a filler with appropriate permeability must play a critical role in maximizing the MMM's separation factor. Figure 9A demonstrates how this filler permeability affects the MMM separation

factor given a constant filler perm-selectivity. For each perm-selectivity exhibited by a filler, a matching permeability yields a maximum separation factor in the resulting MMM. Furthermore, as the filler's perm-selectivity increases, so too does this "optimum" filler permeability.

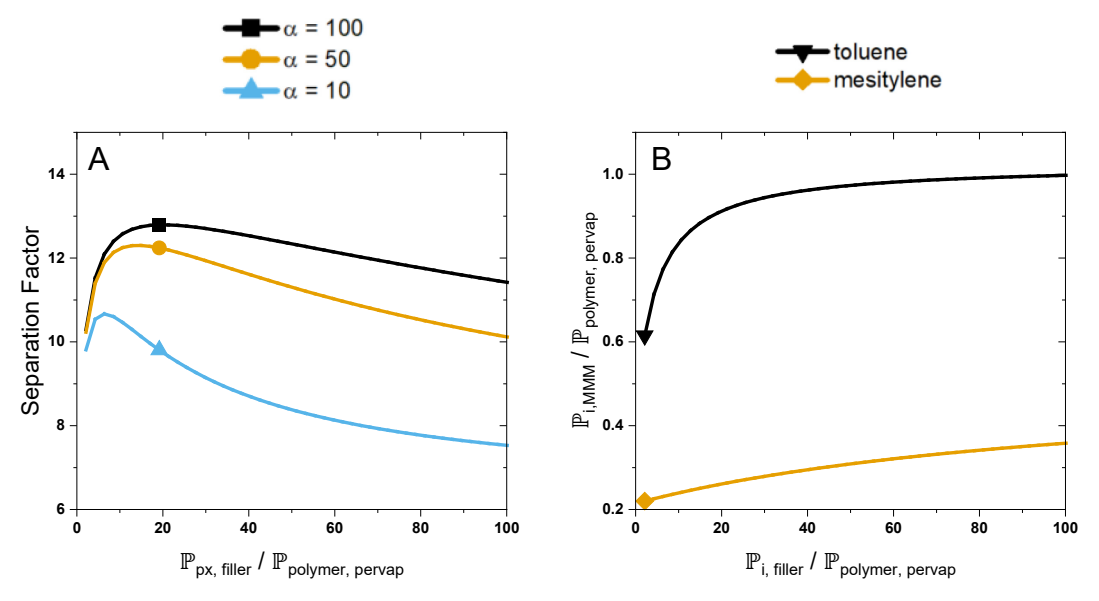


Figure 9: Polymer-filler matching. A) The separation factor of the final MMM at 100 bar of transmembrane pressure shown as a function of polymer-normalized filler permeability for filler pervaporation perm-selectivities of 100, 50, and 10. B) MMM pentrant permeabilities as a function of filler permeability given a pervaporation perm-selectivity of 10

To understand why a specific permeability elicits a maximum separation factor, it is best to recall how the MMM permeability changes as a result of the filler permeability. As the permeability of the filler increases, the MMM permeability increases asymptotically, as shown in Figure 9B. As the filler is very selective for the more permeable species, this species will level off first, while the slow species permeability will intrinsically be closer to the polymer permeability (in this analysis). The two asymptotic MMM permeability responses for the hypothetical toluene and mesitylene permeabilities through a filler material (relative to a pure polymer) are shown in Figure 9B. Initially, this creates a widening spread between the two permeabilities leading to an increasing separation factor. As the filler permeability continues to increase relative to the polymer (for both fast and slow penetrants), the increase of the slower component's MMM permeability matches and then surpasses that of the faster component, leading to the observed downturn in separation factor,

v. OSRO Performance

To qualitatively investigate the validity of the model's findings, dual-layer mixed matrix hollow fiber membranes were fabricated using the pairing of MOF UiO-66 and the polyimide Matrimid®. The hollow fiber membranes were then tested using a 98/2 mol % mixture of toluene and mesitylene, respectively. Chosen for their slight difference in kinetic diameters, the pair of toluene and mesitylene should provide a good measure of OSRO performance. The window size of UiO-

66 lies between these diameters and should therefore serve as a useful sieve for this separation. Figure 10B/C shows SEM images of the fiber exterior and the selective skin layer. Within the skin layer one can clearly see the presence of UiO-66. Images of the fiber exterior demonstrate good dispersion of UiO-66 across the selective skin layer.

A 10 volume percent UiO-66/Matrimid® hollow fiber membrane was compared against a pure Matrimid® hollow fiber membrane. Due to the difficulty fabricating defect-free mixed matrix membranes with higher loadings, only a 10 volume percent membrane was compared to model values in this work.

The membrane test modules were connected in series on a continuous cross-flow unit, described in section 4.5, which allows for multi-day runs while maintaining low stage cuts. To investigate the preceding model findings, the membranes were tested at two pressures. Figure 10A shows the separation factors and permeances measured from the multicomponent separations. A decrease in permeance is observed from 10 to 20 bar of transmembrane pressure, consistent with the solution-diffusion model. As the pressure increases, the separation factors of both membranes increase noticeably. This is a result of an increase in driving force for toluene over mesitylene, and the more pronounced enhancement in separation factor for the MMM is likely a result of the inclusion of UiO-66. Higher loadings and higher pressures of UiO-66 within a Matrimid® matrix will be investigated in future work.

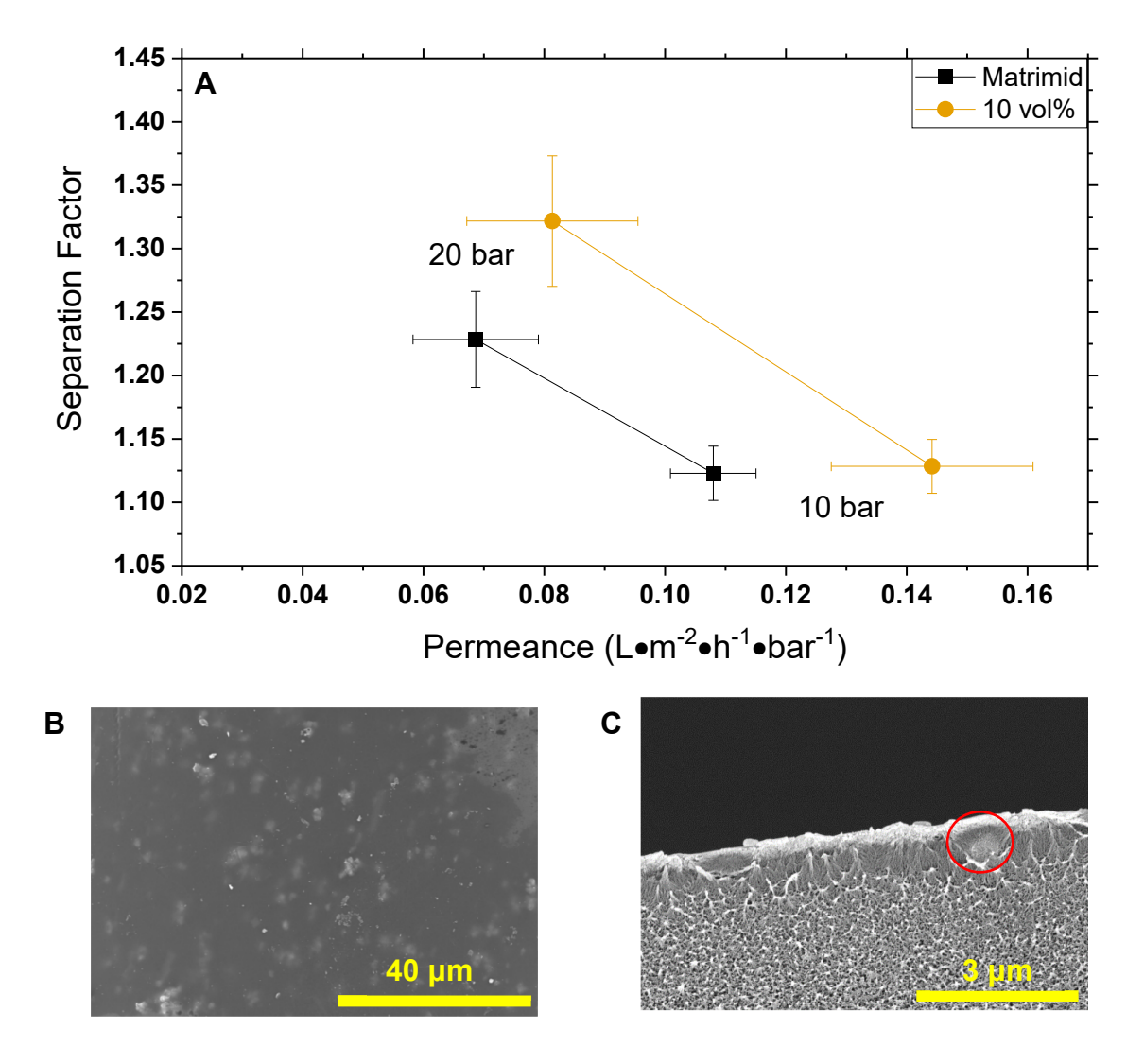


Figure 10: A) Permeance and separation factor of Matrimid hollow fiber membrane and 10 vol% UiO-66/Matrimid hollow fiber membranes with a feed solution of 98/2 mol% toluene/mesitylene. B) The exterior skin layer of the 10 vol% UiO-66/Matrimid® MMM C) Cross-section of skin-layer, porous substructure, and transition region of a 10 vol% UiO-66/Matrimid® fiber. UiO-66 is seen present in the skin layer without noticeable defects (circled in red)

Data collected at 20 bar was chosen for comparison with the mixed matrix membrane transport model. Figure 11 shows the 20 bar results for both the cross-linked Matrimid® and 10 vol% UiO-66 MMM compared against the model predictions for a MMM containing a filler with varied permeability and a specified perm-selectivity. For clarity, the permeabilities have been normalized to the polymer. The separation factor maximums explored earlier in Figure 9 are clearly demonstrated across a range of perm-selectivities here. These maximums shift to the right as the perm-selectivity of the filler increases, showing that the more selective a filler is, the more permeable it must be to fully realize its potential within MMMs.

Focusing on the experimental 10 volume % MMM we see that it lies well within the region of predicted performance for a MMM. As shown in Figure 11, the 10 vol% MMM lies directly on the curve corresponding to a UiO-66 perm-selectivity of 3.9 for the pair of toluene and mesitylene, highlighting qualitative agreement between the experiment and model. We observe an 8% increase in separation factor and an 18% increase in toluene permeance upon inclusion of 10 vol% UiO-66. It is interesting to note that even if the filler exhibited a perm-selectivity of 100 for this pair, an increase of only \sim 1% in separation factor would have been observed, according to our model predictions. This highlights the importance of matrix selectivity in MMM performance.

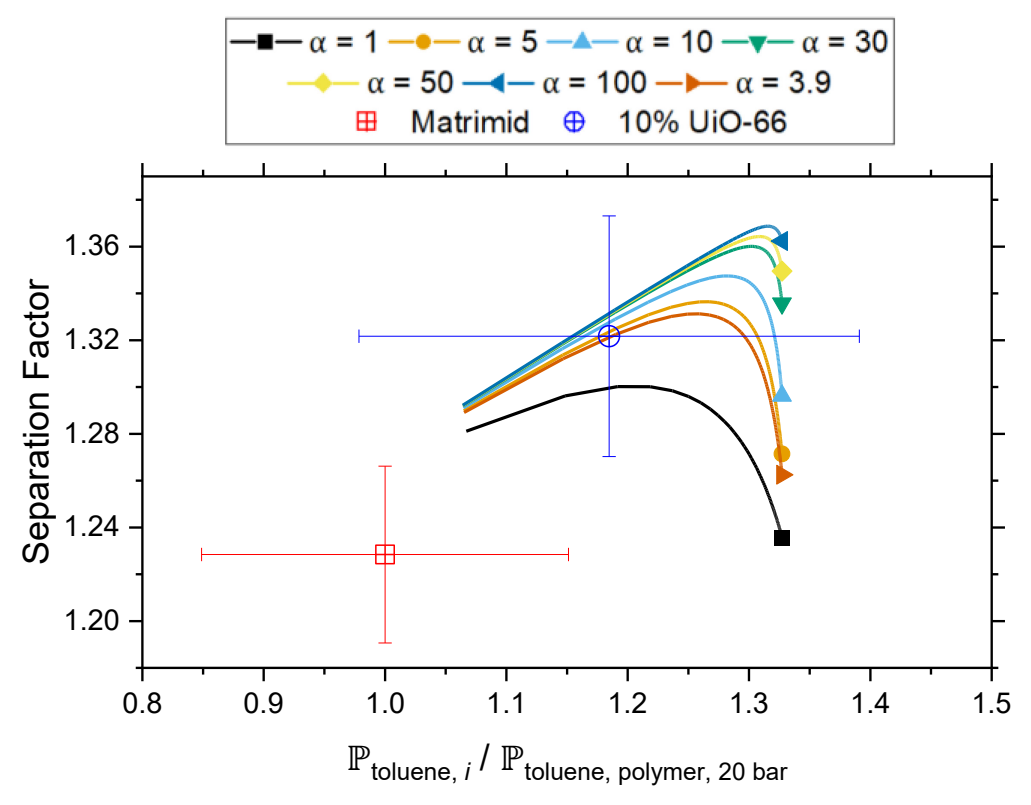


Figure 11: Comparison of experimental results to model predictions for theoretical 10 vol% MMMs at 20 bar. All permeabilities have been normalized to that of the polymer at these conditions. The labels in the legend correspond to the permselectivities of the filler within the MMM as described in Figure 2

6. Conclusions

Proper matching of filler and polymer has been shown as critical to the formation of high-performing MMMs, and OSRO is no exception to this general rule. Our model has determined that there is a unique filler selectivity for each filler permeability that yields the maximum separation factor for the MMM. Unlike previous studies of gas separation MMMs, where optimal filler permeability is usually similar to the polymer's, in solvent separations, the optimal filler permeability increases with filler selectivity. Knowledge of this trend will help in pairing MMM materials across a wide range of potential solvent separations. These membranes also demonstrated

that the MOF UiO-66 is somewhat selective for small solvent molecules and that this selectivity exceeds that of the polyimide Matrimid®.

While this work provides insight into the matching of filler/polymer pairings in MMMs for OSRO separations, some key limitations exist. The experimental work focused on a single pair of materials, UiO-66 and Matrimid®, as well-characterized materials that can be readily acquired and recreated as MMMs in other laboratories. As MMMs continue to develop for OSRO applications, it would be interesting to see how the model demonstrated in this work fairs with other material pairs. Another limitation of this work is the relatively low volume loadings of the MOF in the MMM, which results from the difficulty in fabricating defect-free MMMs at higher volume loadings, and thus the model predictions at higher MOF loadings cannot be validated using the existing data set in this work as well as that of the broader literature.

This experimental and analytical approach reveals that OSRO MMMs for small molecule solvent pairs in which all penetrants to be separated can enter the filler phase are intrinsically disadvantaged relative to gas separation MMMs. The underlying cause of this is the simple fact that most polymer membranes struggle to differentiate between molecules capable of entering into the micropores of typical filler materials (which often have micropores < 10 Å in size), unlike gas separation membranes, which provide greater intrinsic perm-selectivity. This lower baseline requires fillers that are extraordinarily selective and permeable to enable meaningful gains in separation performance. Taken to the limit, this highlights a path forward for OSRO MMMs, which is the utilization of molecular sieves that truly enable size exclusion of certain penetrants relative to others. Fillers such as these will certainly result in positive and transformational impacts on the pure polymer membranes, which is aligned with the longstanding goals of MMMs.

7. Nomenclature

а activity b Langmuir affinity constant (kPa-1) Cmolar concentration (mol•m-3) D Fickian Diffusivity (m²•s⁻¹) Maxwell-Stefan Diffusivity (m2•s-1) Ð f Fugacity (kPa) ŀ membrane thickness (m) phenomenological constant L N Flux ($mol \cdot m^{-2} \cdot s^{-1}$) P Permeability (mol·m·m-2·s-1·Pa-1) molar loading in membrane (mmol•g-1) q S Sorption Component (mol•m-3•Pa) guest velocity (m•s-1) u \bar{V} Partial molar volume (m³•mol⁻¹) mole fraction Χ Distance into membrane (m)

Matrices

| В | Diffusion matrix |
|---|-----------------------------|
| F | dimensionless fugacity |
| N | Matrix of molar fluxes |
| q | diagonal matrix of loadings |

Greek Letters

| α | Perm-selectivity |
|--------|---|
| β | Separation factor |
| δ | ratio of outer interfacial to radius to inner core radius |
| η | dimensionless membrane position |
| θ | fractional occupancy |
| λ | Permeability ratio |
| μ | Chemical potential (J•mol-1) |
| ho | Density (g•m-3) |
| ϕ | Volume fraction |

8. Acknowledgements.

This work was supported by the National Science Foundation (CBET- 1653153), and upon work supported by the U.S. Department of Energy's Office of Energy Efficiency and Renewable Energy (EERE) under the Advanced Manufacturing Office Award Number DE-EE0007888.

9. References

- (1) Brueske, S.; Kramer, C.; Fisher, A. Bandwidth Study on Energy Use and Potential Energy Saving Opportunities in U.S. Petroleum Refining; U.S. Department of Energy Advanced Manufacturing Office: 2015.
- (2) Sholl, D. S.; Lively, R. P., Seven chemical separations to change the world. *Nature* **2016**, *532* (7600), 435-437.
- (3) Materials for Separation Technologies. Energy and Emission Reduction Opportunities; Oak Ridge National Lab. (ORNL), Oak Ridge, TN (United States): 2005; p Medium: ED; Size: 118 p.
- (4) Lipnizki, F.; Field, R. W.; Ten, P.-K., Pervaporation-based hybrid process: a review of process design, applications and economics. *J. Membr. Sci.* **1999**, *153* (2), 183-210.
- (5) Eumine Suk, D.; Matsuura, T., Membrane-Based Hybrid Processes: A Review. *Sep. Sci. Technol. (Philadelphia, PA, U. S.)* **2006,** *41* (4), 595-626.
- (6) Moore, T. T.; Mahajan, R.; Vu, D. Q.; Koros, W. J., Hybrid membrane materials comprising organic polymers with rigid dispersed phases. *AIChE J.* **2004**, *50* (2), 311-321.
- (7) Koros, W. J.; Fleming, G. K., Membrane-based gas separation. *J. Membr. Sci.* **1993**, *83* (1), 1-80.
- (8) Wind, J. D.; Staudt-Bickel, C.; Paul, D. R.; Koros, W. J., The Effects of Crosslinking Chemistry on CO2 Plasticization of Polyimide Gas Separation Membranes. *Ind. Eng. Chem. Res.* **2002**, *41* (24), 6139-6148.
- (9) Staudt-Bickel, C.; J. Koros, W., Improvement of CO2/CH4 separation characteristics of polyimides by chemical cross-linking. *J. Membr. Sci.* **1999**, *155* (1), 145-154.
- (10) Vanherck, K.; Cano-Odena, A.; Koeckelberghs, G.; Dedroog, T.; Vankelecom, I., A simplified diamine cross-linking method for PI nanofiltration membranes. *J. Membr. Sci.* **2010**, 353 (1-2), 135-143.
- (11) Vu, D. Q.; Koros, W. J.; Miller, S. J., Mixed matrix membranes using carbon molecular sieves: I. Preparation and experimental results. *J. Membr. Sci.* **2003**, *211* (2), 311-334.
- (12) Paul, D. R.; Ebra-Lima, O. M., Pressure-induced diffusion of organic liquids through highly swollen polymer membranes. *J. Appl. Polym. Sci.* **1970**, *14* (9), 2201-2224.
- (13) Ma, Y.; Zhang, F.; Yang, S.; Lively, R. P., Evidence for entropic diffusion selection of xylene isomers in carbon molecular sieve membranes. *J. Membr. Sci.* **2018**, *564*, 404-414.
- (14) Thompson, K. A.; Mathias, R.; Kim, D.; Kim, J.; Rangnekar, N.; Johnson, J. R.; Hoy, S. J.; Bechis, I.; Tarzia, A.; Jelfs, K. E.; McCool, B. A.; Livingston, A. G.; Lively, R. P.; Finn, M. G., N-Aryl-linked spirocyclic polymers for membrane separations of complex hydrocarbon mixtures. *Science* **2020**, *369* (6501), 310-315.
- (15) Jang, H.-Y.; Johnson, J. R.; Ma, Y.; Mathias, R.; Bhandari, D. A.; Lively, R. P., Torlon® hollow fiber membranes for organic solvent reverse osmosis separation of complex aromatic hydrocarbon mixtures. *AIChE J.* **2019**, *65* (12), e16757.
- (16) Koh, D.-Y.; McCool, B. A.; Deckman, H. W.; Lively, R. P., Reverse osmosis molecular differentiation of organic liquids using carbon molecular sieve membranes. *Science* **2016**, *353* (6301), 804.
- (17) Darvishmanesh, S.; Tasselli, F.; Jansen, J. C.; Tocci, E.; Bazzarelli, F.; Bernardo, P.; Luis, P.; Degrève, J.; Drioli, E.; Van der Bruggen, B., Preparation of solvent stable polyphenylsulfone hollow fiber nanofiltration membranes. *J. Membr. Sci.* **2011**, *384* (1), 89-96.

- (18) Sun, S.-P.; Chan, S.-Y.; Xing, W.; Wang, Y.; Chung, T.-S., Facile Synthesis of Dual-Layer Organic Solvent Nanofiltration (OSN) Hollow Fiber Membranes. *ACS Sustainable Chem. Eng.* **2015**, *3* (12), 3019-3023.
- (19) Loh, X. X.; Sairam, M.; Steinke, J. H. G.; Livingston, A. G.; Bismarck, A.; Li, K., Polyaniline hollow fibres for organic solvent nanofiltration. *Chem. Commun. (Cambridge, U. K.)* **2008**, (47), 6324-6326.
- (20) Clausi, D. T.; Koros, W. J., Formation of defect-free polyimide hollow fiber membranes for gas separations. *J. Membr. Sci.* **2000**, *167* (1), 79-89.
- (21) Zhang, C.; Zhang, K.; Xu, L.; Labreche, Y.; Kraftschik, B.; Koros, W. J., Highly scalable ZIF-based mixed-matrix hollow fiber membranes for advanced hydrocarbon separations. *AIChE J.* **2014**, *60* (7), 2625-2635.
- (22) Husain, S.; Koros, W. J., Mixed matrix hollow fiber membranes made with modified HSSZ-13 zeolite in polyetherimide polymer matrix for gas separation. *J. Membr. Sci.* **2007**, *288* (1), 195-207.
- (23) Jiang, L. Y.; Chung, T. S.; Cao, C.; Huang, Z.; Kulprathipanja, S., Fundamental understanding of nano-sized zeolite distribution in the formation of the mixed matrix single- and dual-layer asymmetric hollow fiber membranes. *J. Membr. Sci.* **2005**, *252* (1), 89-100.
- (24) Wijmans, J. G.; Baker, R. W., The Solution-Diffusion Model a Review. *J. Membr. Sci.* **1995,** *107* (1-2), 1-21.
- (25) Cheng, C.; Iyengar, S. A.; Karnik, R., Molecular size-dependent subcontinuum solvent permeation and ultrafast nanofiltration across nanoporous graphene membranes. *Nat. Nanotechnol.* **2021**, *16* (9), 989-995.
- (26) Krishna, R.; Wesselingh, J. A., The Maxwell-Stefan approach to mass transfer. *Chem. Eng. Sci.* **1997,** *52* (6), 861-911.
- (27) Bausa, J.; Marquardt, W., Detailed modeling of stationary and transient mass transfer across pervaporation membranes. *AIChE J.* **2001**, *47* (6), 1318-1332.
- (28) Paul, D. R., Reformulation of the solution-diffusion theory of reverse osmosis. *J. Membr. Sci.* **2004**, *241* (2), 371-386.
- (29) Heintz, A.; Stephan, W., A generalized solution—diffusion model of the pervaporation process through composite membranes Part II. Concentration polarization, coupled diffusion and the influence of the porous support layer. *J. Membr. Sci.* **1994**, *89* (1), 153-169.
- (30) Fornasiero, F.; Prausnitz, J. M.; Radke, C. J., Multicomponent Diffusion in Highly Asymmetric Systems. An Extended Maxwell—Stefan Model for Starkly Different-Sized, Segment-Accessible Chain Molecules. *Macromolecules (Washington, DC, U. S.)* **2005**, *38* (4), 1364-1370.
- (31) Ribeiro, C. P.; Freeman, B. D.; Paul, D. R., Modeling of multicomponent mass transfer across polymer films using a thermodynamically consistent formulation of the Maxwell–Stefan equations in terms of volume fractions. *Polymer* **2011**, *52* (18), 3970-3983.
- (32) Krishna, R., Describing mixture permeation across polymeric membranes by a combination of Maxwell-Stefan and Flory-Huggins models. *Polymer* **2016**, *103*, 124-131.
- (33) Mathias, R.; Weber, D. J.; Thompson, K. A.; Marshall, B. D.; Finn, M. G.; Scott, J. K.; Lively, R. P., Framework for predicting the fractionation of complex liquid feeds via polymer membranes. *J. Membr. Sci.* **2021**, *640*, 119767.
- (34) Keil, Frerich J.; Krishna, Rajamani; Coppens, Marc-Olivier, Modeling of Diffusion in Zeolites. *Rev. Chem. Eng.* **2000**, *16* (2), 71-197.

- (35) Kapteijn, F.; Moulijn, J. A.; Krishna, R., The generalized Maxwell–Stefan model for diffusion in zeolites:: sorbate molecules with different saturation loadings. *Chem. Eng. Sci.* **2000**, 55 (15), 2923-2930.
- (36) Ma, Y.; Zhang, F.; Deckman, H. W.; Koros, W. J.; Lively, R. P., Flux Equations for Osmotically Moderated Sorption–Diffusion Transport in Rigid Microporous Membranes. *Ind. Eng. Chem. Res.* **2020**, *59* (12), 5412-5423.
- (37) Krishna, R.; Baur, R., Analytic solution of the Maxwell–Stefan equations for multicomponent permeation across a zeolite membrane. *Chem. Eng. J. (Amsterdam, Neth.)* **2004,** 97 (1), 37-45.
- (38) Henis, J. M. S.; Tripodi, M. K., Composite hollow fiber membranes for gas separation: the resistance model approach. *J. Membr. Sci.* **1981**, *8* (3), 233-246.
- (39) Monsalve-Bravo, G.; Bhatia, S., Modeling Permeation through Mixed-Matrix Membranes: A Review. *Processes* **2018**, *6* (9), 172.
- (40) Zimmerman, C. M.; Singh, A.; Koros, W. J., Tailoring mixed matrix composite membranes for gas separations. *J. Membr. Sci.* **1997**, *137* (1), 145-154.
- (41) Moore, T. T.; Koros, W. J., Non-ideal effects in organic—inorganic materials for gas separation membranes. *J. Mol. Struct.* **2005**, *739* (1), 87-98.
- (42) Mahajan, R.; Koros, W. J., Mixed matrix membrane materials with glassy polymers. Part 1. *Polym. Eng. Sci.* **2002**, *42* (7), 1420-1431.
- (43) Felske, J. D., Effective thermal conductivity of composite spheres in a continuous medium with contact resistance. *Int. J. Heat Mass Transfer* **2004**, *47* (14), 3453-3461.
- (44) Erucar, I.; Keskin, S., Computational Methods for MOF/Polymer Membranes. *Chem. Rec.* **2016,** *16* (2), 703-718.
- (45) Shimekit, B.; Mukhtar, H.; Murugesan, T., Prediction of the relative permeability of gases in mixed matrix membranes. *J. Membr. Sci.* **2011**, *373* (1), 152-159.
- (46) Hines, A. L. M., Robert N., *Mass Transfer Fundamentals and Applications*. Prentice-Hall: New Jersey, 1985.
- (47) Krishna, R.; Baur, R., Modelling issues in zeolite based separation processes. *Sep. Purif. Technol.* **2003**, *33* (3), 213-254.
- (48) Hwang, S.-T., Non-equilibrium thermodynamics of membrane transport. *AIChE J.* **2004**, *50* (4), 862-870.
- (49) Curtiss, C. F.; Bird, R. B., Multicomponent Diffusion. *Ind. Eng. Chem. Res.* **1999**, *38* (7), 2515-2522.
- (50) Ma, C.; Koros, W. J., Ester-Cross-linkable Composite Hollow Fiber Membranes for CO2 Removal from Natural Gas. *Ind. Eng. Chem. Res.* **2013**, *52* (31), 10495-10505.
- (51) Jang, H. Y.; Lively, R. P., The role of skin layer defects in organic solvent reverse osmosis membranes. *J. Membr. Sci. Lett.* **2021**, *1* (1), 100004.
- (52) Vanherck, K.; Vandezande, P.; Aldea, S. O.; Vankelecom, I. F. J., Cross-linked polyimide membranes for solvent resistant nanofiltration in aprotic solvents. *J. Membr. Sci.* **2008**, *320* (1), 468-476.
- (53) Liu, Y.; Wang, R.; Chung, T.-S., Chemical cross-linking modification of polyimide membranes for gas separation. *J. Membr. Sci.* **2001**, *189* (2), 231-239.
- (54) Cao, C.; Chung, T.-S.; Liu, Y.; Wang, R.; Pramoda, K. P., Chemical cross-linking modification of 6FDA-2,6-DAT hollow fiber membranes for natural gas separation. *J. Membr. Sci.* **2003**, *216* (1), 257-268.

- (55) Jue, M. L.; Koh, D.-Y.; McCool, B. A.; Lively, R. P., Enabling Widespread Use of Microporous Materials for Challenging Organic Solvent Separations. *Chem. Mater.* **2017**, *29* (23), 9863-9876.
- (56) Mahajan, R.; Koros, W. J., Factors Controlling Successful Formation of Mixed-Matrix Gas Separation Materials. *Ind. Eng. Chem. Res.* **2000**, *39* (8), 2692-2696.